Editor-in-Chief: Robert A. Laudise • Associate Editors: Shigeyuki Sōmiya, Heinrich J. Wollenberger

Volume 12. Number 5

Abstracts for May 1997 Journal of Materials Research

TABLE OF CONTENTS

COMMUNICATIONS

Boron diffusion into diamond under electric bias T. Sung, G. Popovici, M.A. Prelas, R.G. Wilson, S.K. Loyalka

The synthesis of NbSi₂ by mechanical alloying T. Lou, G. Fan, B. Ding, Z. Hu

Hydrothermal synthesis of heteroepitaxial Pb(Zr_xTi_{1-x}) O_3 thin films at 90–150°C

A.T. Chien, J.S. Speck, F.F. Lange

Excimer laser deposition of c-axis oriented Pb(Zr,Ti)O₃ thin films on silicon substrates with direct-current glow discharge L. Zheng, X. Hu, P. Yang, W-P. Xu, C. Lin

D.C. electrical conductivity of Versicon™ blended in poly(viny) chloride)
R. Speel, P.K. LeMaire

The syntheses of SiC_p/Al nanocomposites under high pressure H. Liu, A. Wang, L. Wang, B. Ding, Z. Hu, H. Peng

The origin of an anomalous, low 2⊖ peak in x-ray diffraction spectra of MoS₂ films grown by ion beam assisted deposition D.N. Dunn, L.E. Seitzman, I.L. Singer

ARTICLES

Crystalline phases and electronic structures in superconducting Bi-Sr-Ca-Cu oxides

M.D. Giardina, R. Feduzi, D. Inzaghi, A. Manara, C. Giori, I.N. Sora, V. Dallacasa

Raman microscopy examination of phase evolution in Bi(Pb)-Sr-Ca-Cu-O superconducting ceramics

K.T. Wu, A.K. Fischer, V.A. Maroni, M.W. Rupich

Two-stage sintering of dense superconducting $YBa_2Cu_4O_8$ ceramics M. Matsuda, Y. Ogawa, K. Yamashita, T. Umegaki, M. Miyake

Single crystal growth of cuprates from hydroxide fluxes S.A. Sunshine, T. Siegrist, L.F. Schneemeyer

Thin films for superconducting electronics. Precursor performance issues, deposition mechanisms, and superconducting phase formation-processing strategies in the growth of ${\rm TI}_2{\rm Ba}_2{\rm CaCu}_2{\rm O}_8$ films by metal-organic chemical vapor deposition

B.J. Hinds, R.J. McNeely, D.B. Studebaker, T.J. Marks, T.P. Hogan, J.L. Schindler, C.R. Kannewurf, X.F. Zhang, D.J. Miller

Optimizing diamond growth for an atmospheric oxyacetylene torch

L.A. Zeatoun, P.W. Morrison Jr.

Development of a submicrometer-grained microstructure in aluminum 6061 using equal channel angular extrusion

S. Ferrasse, V.M. Segal, K.T. Hartwig, R.E. Goforth

Optical properties of potassium acid phthalate

D. Comoretto, L. Rossi, A. Borghesi

Graphite encapsulated nanocrystals produced using a low carbon:metal ratio

J.J. Host, M.H. Teng, B.R. Elliott, J-H. Hwang, T.O. Mason, D.L. Johnson, V.P. Dravid

Synthesis and properties of an aluminum nitride/polyimide nanocomposite prepared by a nonaqueous suspension process X. Chen, K.E. Gonsalves

Evaluation of a porous fiber coating in SiC-Si $_3$ N $_4$ minicomposite L.U.J.T. Ogbuji

Domain structure of epitaxial PbTiO $_3$ films grown on vicinal (001) ${\rm SrTiO}_3$

C.D. Theis, D.G. Schlom

Heteroepitaxial growth of lanthanum aluminate films derived from mixed metal nitrates

M.F. Ng, M.J. Cima

Phase formation in molybdenum distilicide powders during in-flight induction plasma treatment

X. Fan, T. Ishigaki, Y. Sato

Phase-formation kinetics of xerogel and electrical properties of sol-gel-derived $\text{Ba}_{x}\text{Sr}_{1-x}\text{TiO}_{3}$ thin films

S-I. Jang, B-C. Choi, H.M. Jang

The ballistic failure mechanisms and sequence in semi-infinite supported alumina tiles

D. Sherman, D.G. Brandon

Hot filament assisted diamond growth at low temperatures with oxygen addition

Z.L. Tolt, L. Heatherly, R.E. Clausing, C.S. Feigerle

Nucleation and growth of oriented diamond on Si(100) by bias-assisted chemical vapor deposition

M. Nishitani-Gamo, T. Ando, K. Yamamoto, P.A. Dennig, Y. Sato

JMR Abstracts provides a listing of preliminary titles and abstracts tentatively scheduled to appear in the corresponding issue of Journal of Materials Research. Copyright 1997 by the Materials Research Society. All rights reserved. Although every effort is taken to provide accurate contents here, late schedule changes in Journal of Materials Research may result in articles being rescheduled for later issues or in the addition of late articles to an issue that may not be shown here. The Materials Research Society regrets any inconvenience that may result from late schedule changes. ISSN: 1066-2375.

MRS BULLETIN/MARCH 1997 85

Nitrogen plasma source ion implantation for corrosion protection of aluminum 6061-T4

J.H. Booske, L. Zhang, W. Wang, K. Mente, N. Zjaba, C. Baum, J.L. Shohet

Excess Li ions in a small graphite cluster

M. Nakadaira, R. Saito, T. Kimura, G. Dresselhaus, M.S. Dresselhaus

Surface and bulk characterization of Rh/ZrO_2 prepared by absorption of $Rh_a(CO)_{12}$ clusters on ZrO_2 powder

L.E. Depero, R. Bertoncello, T. Boni, P. Levrangi, I.N. Sora, E. Tempesti, F. Parmigiani

Vapor-deposited CaWO₄ phosphor

P.F. Carcia, M. Reilly, C.C. Torardi, M.K. Crawford, C.R. Miao, B.D. Jones

Effect of lattice mismatch on the epitaxy of sol-gel LiNb03 thin films T.A. Derouin, C.D.E. Lakeman, X.H. Wu, J.S. Speck, F.F. Lange

Lattice site and photoluminescence of erbium implanted in α -Al $_2$ 0 $_3$ G.N. van den Hoven, A. Polman, E. Alves, M.F. da Silva, A.A. Melo, J.C. Soares

Spectroscopic study of Na-TCNQ in a poly (ethylene oxide) matrix $[TCNQ = 7,7^{\circ},8,8^{\circ}$ tetracyanoquinodimethane]

A. Arena, G. Di Marco, M. Lanza, S. Patané, G. Saitta

Agglomeration of silica spheres under ultrasonication

N. Enomoto, S. Maruyama, Z. Nakagawa

ABSTRACTS

COMMUNICATIONS

Boron diffusion into diamond under electric bias

T. Sung*, G. Popovici*, M.A. Prelas*, R.G. Wilson+, S.K. Loyalka* (*University of Missouri-Columbia, +Hughes Research Laboratories)

Three natural type IIa diamond crystals were used for forced diffusion of boron. The diffusion was performed under bias otherwise with the same conditions. The boron diffusion coefficient in diamond was found to be 8.4×10^{-15} at a and 4×10^{-14} cm²/sec at 1000° C, depending on the direction of the electric field. The drift velocity of boron in diamond under 850 V at 1000° C was found to be about 1.2×10^{-8} cm/sec.

Order No.: JA705-001 © 1997 MRS

The synthesis of NbSi₂ by mechanical alloying

T. Lou, G. Fan, B. Ding, Z. Hu (Academia Sinica)

The stoichiometric intermetallic compound $NbSi_2$ has been synthesized by mechanical alloying (MA) elemental Nb and Si powders. The alloying process has been investigated by means of x-ray diffraction (XRD) and differential scanning calorimetry (DSC). It was found that the formation of the Nb_2Si intermetallic compound occurs abruptly after 65 min of milling without any interruptions during the alloying process. However, short interruptions at a 5 min interval during ball milling result in a gradual reaction for the formation of the $NbSi_2$ compound as well as a new metastable bcc structured solid solution. We conclude that the temperature rise during mechanical alloying plays an important role in initiating the abrupt reaction after an incubation milling time.

Order No.: JA705-002 © 1997 MRS

Hydrothermal synthesis of heteroepitaxial Pb(Zr $_{\rm x}$ Ti $_{\rm 1-x}$)0 $_{\rm 3}$ thin films at 90–150°C

A.T. Chien, J.S. Speck, F.F. Lange (University of California-Santa Barbara)

Pb(Zr_xTi_{1-x}) O_3 and Pb ZrO_3 heteroepitaxial thin films were produced in an aqueous solution (10M KOH) at ambient pressure and low temperatures (90–150°C) on (001) Sr TiO_3 and LaAlO $_3$ single crystal substrates. Growth of the Pb(Zr_xTi_{1-x}) O_3 and Pb ZrO_3 thin films initiates by the formation of (100) faceted islands. EDS analysis of the Pb(Zr_xTi_{1-x}) O_3 thin film shows that the Zr:Ti ratio is 44:56, nearly identical to the molar ratio of the precursors. This route might provide a viable low temperature alternative for the formation of high dielectric constant thin films for applications such as dynamic random access memory (DRAM).

Order No.: JA705-003 © 1997 MRS

Excimer laser deposition of c-axis oriented Pb(Zr,Ti) $\mathbf{0}_3$ thin films on silicon substrates with direct-current glow discharge

L. Zheng, X. Hu, P. Yang, W-P. Xu, C. Lin (Chinese Academy of Sciences)

Ferroelectric thin films of Pb(Zr,Ti)O₃ (PZT) were fabricated on platinum coated silicon using the process of direct-current glow discharge assisted laser deposition, where the substrate was electrically grounded. The films deposited at 730°C with +800 V discharge voltage are oriented mostly with the c-axis perpendicular to the substrate surface, and exhibit good ferroelectric hysteresis loops. A possible mechanism for the improvement of the deposition process has been proposed.

Order No.: JA705-004 © 1997 MRS

D.C. electrical conductivity of Versicon™ blended in poly(vinyl chloride)

R. Speel, P.K. LeMaire

(Central Connecticut State University)

The D.C. electrical conductivity of the conducting polymer Versicon™ blended in poly(vinyl chloride) (PVC) was measured from 25 K to 310 K. The data was fitted to various electrical transport models and the best fit was found with the fluctuation-induced tunneling model, suggesting that tunneling dominates in the mode of electron transport at low temperatures. The parameters, T₁ and T₀ from the fluctuation-induced tunneling model, were found to be 625 K and 129 K, respectively. The inter-particle distance was estimated to be about 13 Å. At higher temperatures, the plot of the log of resistivity versus the reciprocal of the temperature was linear, indicating that thermally activated hopping dominated the mode of electrical transport at these temperatures. The results support earlier findings that Versicon™ forms continuous aggregates in blends. The results also support growing evidence in the literature that these types of aggregate formation tend to strongly influence the mode of electrical transport in composites.

Order No.: JA705-005 © 1997 MRS

The syntheses of SiC_p/Al nanocomposites under high pressure H. Liu, A. Wang, L. Wang, B. Ding, Z. Hu, H. Peng (Academia Sinica)

The SiC_p/Al nanocomposites were synthesized under high pressure. The reaction behavior between SiC particles and Al matrix within 2–6 GPa pressure range was determined. The HREM observation and the Vickers microhardness measurement show that the reaction is slight and that the adhesion of SiC particles to the Al matrix is good whether the reaction between them occurred or not. This offered an opportunity to tailor the

nanocomposites' mechanical properties by adjusting the synthesis temperature, pressure and volume fraction of SiC particles.

Order No.: JA705-006 © 1997 MRS

The origin of an anomalous, low 2Θ peak in x-ray diffraction spectra of MoS₂ films grown by ion beam assisted deposition

D.N. Dunn, L.E. Seitzman, I.L. Singer (Naval Research Laboratory)

The origin of a previously reported anomalous low 2Θ x-ray diffraction peak from MoS_2 thin films grown by ion beam assisted deposition was investigated. The anomalous peak, observed in a film grown on Si(100), was removed by ion irradiating the film with 180 keV Ar*+ ions to a dose of 1 x 10^{15} ions/cm². Microstructures of the two films were investigated using x-ray diffraction and cross section transmission electron microscopy. Diffraction data and bright field images indicated that the low 2Θ peak was due to a local interplanar expansion of the crystal structure normal to MoS_2 basal planes. Expansion was attributed to molecular defects.

Order No.: JA705-007 © 1997 MRS

ARTICLES

Crystalline phases and electronic structures in superconducting Bi-Sr-Ca-Cu oxides

M.D. Giardina*, R. Feduzi*, D. Inzaghi*, A. Manara*, C. Giori+, I.N. Sora#, V. Dallacasa§

(*Institute for Advanced Materials-C.E.C. Joint Research Centre, +Università di Parma, #Università di Brescia, \$Università di Verona)

Two classes of samples, called A and B, of layered Bi-Sr-Ca-Cu oxides having the same nominal composition 4:3:3:4 were investigated by using microwave absorption (EPR), powder x-ray diffraction (XRD), x-ray photoelectric spectroscopy (XPS), and x-ray absorption near edge structure (XANES). Previous electrical resistivity measurements had shown that only the B-samples presented two superconducting phases at about 80 and 106 K. The microwave absorption technique instead indicated the presence of superconducting islands at the above-mentioned temperatures also in the A-samples. The crystalline and electronic structures of the two types of samples are illustrated and discussed. A plausible theoretical interpretation of the experimental results is given, based on a quantum percolation model with Coulomb interaction.

Order No.: JA705-008 © 1997 MRS

Raman microscopy examination of phase evolution in Bi(Pb)-Sr-Ca-Cu-O superconducting ceramics

K.T. Wu*, A.K. Fischer*, V.A. Maroni*, M.W. Rupich*

(*Argonne National Laboratory, +American Superconductor Corporation) Raman microspectroscopy (RMS) and imaging Raman microscopy (IRM) were used to probe the composition and spatial distribution of chemical phases in Bi(Pb)-Sr-Ca-Cu-O (BSCCO) ceramic superconductor powders and silver-BSCCO composites. The Raman techniques were used to identify various phases, including alkaline earth cuprates, CuO Bi-2212, Bi-2223, and Pb-containing phases. Changes in the Ca/Sr ratios in (Ca,Sr)₂CuO₃ phases were distinguished by orientational differences with respect to polarization of the exciting radiation. Variations were observed in the content and distribution of lead in various phases formed during intermediate stages of the thermal processing of composite conductors. The spatial distribution of the various phases detected in powder and composite conductors was established to a-resolution of a few microns by collecting images of the Raman scattering at wavelengths corresponding to the signature peaks of the observed phases. Reference Raman spectra of the major phases observed in the BSCCO system are also reported. The Raman techniques, when combined with complimentary techniques, such as x-ray diffraction and electron microscopy, can provide valuable information about the reaction paths and mechanisms of the high temperature BSCCO superconducting ceramics.

Order No.: JA705-009 © 1997 MRS

Two-stage sintering of dense superconducting YBa₂Cu₄O₈ ceramics M. Matsuda*, Y. Ogawa*, K. Yamashita*, T. Umegaki*, M. Miyake* (*Tokyo Metropolitan University, *Okayama University)

Dense YBa₂Cu₄O₈ (124) ceramics were prepared by the following two-stage sintering; compressed 124 powders were heated to 1203 K for decomposition to YBa₂Cu₃O_{7-x} (123) and CuO, and then cooled down to 1073 K and annealed for the reformation of 124 single phase. The relative densities thus obtained were 93–95%, as high as those prepared under high oxygen pressure. The densification was considered to take place due to liquid phase. In the sintered 124, the island-like fine grains of CuO were observed within the 123 matrix. As a result, it was considered that the reformation of 124 proceeded in each grain. The geometrical phase distribution in the grains was discussed on the basis of superconducting properties from resistivity measurements.

Order No.: JA705-010 © 1997 MRS

Single crystal growth of cuprates from hydroxide fluxes S.A. Sunshine, T. Siegrist, L.F. Schneemeyer (Bell Laboratories-Lucent Technologies)

Barium and potassium hydroxide have been investigated as fluxes for the growth of cuprate single crystals. The relatively high solubility of transition metals and lanthanoids in these salt fluxes at moderate temperatures allows significant lowering of the growth temperatures required for many phases. Also, phases not stable at high temperatures become accessible. Two new cuprates have been prepared in the Ba-Ca-Cu-O and Ba-Y-Cu-O systems from a Ba(OH) $_2 \cdot H_2O$ flux. The compounds Ba $_3(Y_{0.23}Cu_{0.77})_2O_{5.78}$ and Ba $_3(Ca_{0.24}Cu_{0.76})_2O_{4.43}$ crystallize in a tetragonal (space group I4/mmm) oxygen deficient Sr $_3Ti_2O_7$ -type structure with lattice parameters a = 4.069 (2) Å, 4.022 (1) Å and c = 21.61 (2) Å, 21.63 (2) Å, respectively. The compound (Ba $_{0.92}Sr_{0.08})$ (Ca $_{0.38}Cu_{0.62})O_{2.1}$ crystallizes with a doubled perovskite unit cell along all three axes, a = 8.116 (4) Å. In addition, single crystals of Ba $_2YCu_3O_{7-\delta}$ have been prepared from a KOH flux at 750°C. **Order No.: JA705-011**

Thin films for superconducting electronics. Precursor performance issues, deposition mechanisms, and superconducting phase formation-processing strategies in the growth of ${\rm Tl_2Ba_2CaCu_2O_8}$ films by metal-organic chemical vapor deposition

B.J. Hinds*, R.J. McNeely*, D.B. Studebaker*, T.J. Marks*, T.P. Hogan*, J.L. Schindler*, C.R. Kannewurf*, X.F. Zhang*, D.J. Miller* (*Northwestern University, *Argonne National Laboratory)

Epitaxial Tl₂Ba₂CaCu₂O₈ thin films with excellent electrical transport characteristics are grown in a two-step process involving metal-organic chemical vapor deposition (MOCVD) of a BaCaCuO(F) thin film followed by a post-anneal in the presence of TI₂O vapor. Vapor pressure characteristics of the recently developed liquid metal-organic precursors Ba(hfa)₂·mep (hfa = hexafluoroacetylacetonate, mep = methylethylpentaglyme), Ca(hfa)2 tet (tet = tetraglyme), and the solid precursor Cu(dpm)₂ (dpm = dipivaloylmethanate) are characterized by low pressure thermogravimetric analysis. Under typical film growth conditions, transport is shown to be diffusion-limited. The transport rate of Ba(hfa)2-mep is demonstrated to be stable for over 85 h at typical MOCVD temperatures (120°C). In contrast, the vapor pressure stability of the commonly used Ba precursor, Ba(dpm)2, deteriorates rapidly at typical growth temperatures, and the decrease in vapor pressure is approximately exponential with a half-life of ~9.4 hr. These precursors are employed in a low pressure (5 Torr) horizontal, hot-wall, film growth reactor for growth of BaCaCuO(F) thin films on (110) LaAlO₃ substrates. From the dependence of film deposition rate on substrate temperature and precursor partial pressure, the kinetics of deposition are shown to be mass-transport limited over the temperature range 350-650°C at a 20 nm/min deposition rate. A ligand exchange process which yields volatile Cu(hfa), and Cu(hfa)(dpm) is also observed under film growth conditions. The MOCVD derived BaCaCuO(F) films are post-annealed in the presence of bulk Tl₂Ba₂CaCu₂O₈ at temperatures of 720-890°C in flowing atmospheres ranging from 0–100% O_2 . The resulting $Tl_2Ba_2CaCu_2O_8$ films are shown to be epitaxial by x-ray diffraction and TEM analysis with the c-axis normal to the substrate surface, with in-plane alignment, and with abrupt film-substrate interfaces. The best films exhibit a T_c = 105 K, transport-measured J_c = 1.2 x 10⁵ A/cm² at 77 K, and surface resistances as low as 0.4 m Ω (40 K, 10 GHz).

Order No.: JA705-012

© 1997 MRS

Optimizing diamond growth for an atmospheric oxyacetylene torch L.A. Zeatoun, P.W. Morrison Jr.

(Case Western Reserve University)

Diamond growth conditions for an atmospheric combustion flame have been optimized using statistical experimental design. Films are grown on a molybdenum bolt for 40 minutes at a distance of 1 mm from the flame cone. The diamond films have been characterized using Raman spectroscopy, x-ray diffraction, and scanning electron microscope.

The input process variables are varied over a range of conditions: total gas flow rate Q = 2–4 standard liter/min, substrate surface temperature T_s = 800–1000°C, and flow ratio of O_2/C_2H_2 = R = 0.93–0.99. The experimental response outputs are growth rate, full width half maximum (FWHM) of the diamond Raman peak, Raman diamond fraction (β) in the film, ratio of luminescence to diamond peak height (LR), and the relative intensity of the {220}, {311}, {400}, and {331} orientations. The film quality indices FWHM, β , and LR improve by increasing the gas ratio (R), by increasing substrate surface temperature (T_s), and lowering the growth rate by decreasing total gas flow rate. Diamond film shows a small amount texturing in {220} and {400} orientation at low R and T_s . At high R and low T_s , crystals are oriented with the {111} direction normal to the substrate surface.

Jet and boundary layer theory have been applied to understand the growth rate, the thickness profile, and the morphological instability of the diamond films. Surface Damköhler calculation shows that the deposition process is marginally controlled by mass transfer. Growth rate of an open flame is higher than for an enclosed flame, while the Raman quality measurements of the enclosed flame are more uniform than open flame over the range of the comparison.

Order No.: JA705-013

© 1997 MRS

Development of a submicrometer-grained microstructure in aluminum 6061 using equal channel angular extrusion

S. Ferrasse*, V.M. Segal*, K.T. Hartwig*, R.E. Goforth* (*Texas A&M University, *Johnson Matthey)

Submicrometer-grained (SMG) microstructures are produced in an Al-Mg-Si alloy (6061) by subjecting peak-aged and overaged billets of the alloy to intense plastic strain by a process known as equal channel angular extrusion. Two types of refined structure are distinguished by optical and transmission electron microscopy. One structure is created through intense deformation (four extrusion passes through a 90° die, $\epsilon=4.68$) by dynamic rotational recrystallization and is a well-formed grain (fragmented) structure with a mean fragment or grain size of 0.2–0.4 μm . The other structure is produced by post-extrusion annealing through static migration recrystallization resulting in a grain size of 5–15 μm . Intense deformation of peak-aged material to a true strain ϵ of 4.68 (four passes) produces a strong, ductile, uniform, fine and high angle grain boundary microstructure with increased stability against static recrystallization as compared to the overaged material.

Order No.: JA705-014

© 1997 MRS

Optical properties of potassium acid phthalate

D. Comoretto*, L. Rossi+, A. Borghesi*

(*Università degli Studi di Genova, +Università degli Studi di Pavia, #Università degli Studi di Modena)

Potassium acid phthalate (KAP) crystals are promising as substrates for the growth of highly oriented films of conjugated polymers with exceedingly high and fast non-linear optical response.

We report the KAP optical properties (real and imaginary parts of the refractive index $\tilde{n}=n+ik$) in the near infrared and visible range

deduced by ellipsometric measurements and direct inversion of transmittance and near-normal incidence absolute reflectance measurements. In the infrared region n was also deduced by the interference fringes.

Order No.: JA705-015

© 1997 MRS

Graphite encapsulated nanocrystals produced using a low carbon:metal ratio

J.J. Host, M.H. Teng, B.R. Elliott, J-H. Hwang, T.O. Mason, D.L. Johnson, V.P. Dravid (Northwestern University)

Graphite encapsulated nanocrystals produced by a low carbon tungsten arc were analyzed to determine their chemistry, crystallography and nanostructural morphology. Metallic nanocrystals of Fe, Co and Ni are in the FCC phase, and no trace of the bulk equilibrium phases of body centered cubic (Fe) and hexagonal close-packed (Co) were found. Various analytical techniques have revealed that the encased nanocrystals are pure metal (some carbide was found in the case of Fe), ferromagnetic, and generally spherical. The nanocrystals are protected by turbostratic graphite, regardless of the size of the nanocrystals. The turbostratic graphite coating is usually made up of between 2 and 10 layers. No trace of any unwanted elements (e.g., oxygen) was found. The low carbon: metal ratio arc technique is a relatively clean process for the production of graphite encapsulated nanocrystals.

Order No.: JA705-016

© 1997 MRS

Synthesis and properties of an aluminum nitride/polyimide nanocomposite prepared by a nonaqueous suspension process X. Chen, K.E. Gonsalves

(University of Connecticut)

A nanocomposite of a chemically synthesized nanostructured aluminum nitride (AIN) and a polyimide has been studied. Using a nonaqueous polar solvent, N-methylpyrrolidinone (NMP), as the suspension media, the degree of particle agglomeration of AIN was reduced dramatically from micron to nanoscale size. Upon the addition of poly(amic acid) to the AIN/NMP suspension, a further deagglomeration of the particles was observed. The surface physicochemical interactions have been investigated by characteristic model reactions using FTIR spectroscopy. A mechanistic interpretation for the deagglomeration and stabilization behavior are discussed. The formation of the AIN/PI nanocomposite was achieved by the rapid solidification of the precursor suspension followed by compression molding. Such an approach for nanocomposites exhibits better homogeneity with ultrafine fillers and allows a tailorable composition and property at the nanoscale level. Finally, AIN/PI nanocomposites with an increased ceramic loading, up to 65% by volume, were attained and their thermal and mechanical properties, along with the compositional effects, have been investigated.

Order No.: JA705-017

© 1997 MRS

Evaluation of a porous fiber coating in $SiC-Si_3N_4$ minicomposite L.U.J.T. Ogbuji

(NASA-Lewis Research Center)

A porous and discontinuous $\mathrm{Si_3N_4}$ -based fiber coating was evaluated in $\mathrm{SiC/Si_3N_4}$ minicomposites by fiber push-out and fractography for debond capabilities following high-temperature exposures. The exposures consisted of 500 h annealing at 1350°C, and 25–100 h oxidation in wafer form at 1200–1400°C. In spite of considerable microstructural coarsening and/or oxidation of the coating, fiber debond and sliding were achieved in all cases, and at stress levels comparable to those reported for tough, as-fabricated $\mathrm{SiC/Si_3N_4}$ composites with a carbon or boron nitride interphase. Therefore, the porous coating is expected to perform better than C or BN in applications where oxidation is inevitable. The role of porosity in accommodating and mitigating the effects of oxidation is thought to be important.

Order No.: JA705-018

© 1997 MRS

Domain structure of epitaxial PbTiO $_3$ films grown on vicinal (001) SrTiO $_3$

C.D. Theis, D.G. Schlom

(The Pennsylvania State University)

Epitaxial PbTiO₃ films have been grown on vicinal (001) SrTiO₃ substrates by pulsed laser deposition. Vicinal SrTiO₃ substrates with misorientations up to 9° from (001) were used and the influence of the direction of misorientation on the resulting domain structure was studied. 4-circle x-ray diffraction analysis indicates that thin (40 nm) PbTiO₃ films are completely c-axis oriented (rocking curve FWHM of 0.25° for the 002 reflection) and that thicker films (~200 nm) contain mixed a-axis and c-axis PbTiO₃ domains due to twinning along {011} planes. The [100] axis of the a-axis domains are misoriented by 2.1° to 3.3° toward <100> substrate directions with respect to the substrate normal. In contrast to growth on well-oriented (001) SrTiO₃ surfaces where the four equivalent tilts of the [100] axis of the a-axis domains are equally likely, on vicinal SrTiO₃ the a-axis domains are preferentially oriented in an uphill direction with respect to the crystallographic miscut.

Order No.: JA705-019 © 1997 MRS

Heteroepitaxial growth of lanthanum aluminate films derived from mixed metal nitrates

M.F. Ng, M.J. Cima

(Massachusetts Institute of Technology)

Epitaxial lanthanum aluminate (LaAlO₃) thin films were deposited on single-crystal substrates by pyrolysis of spin-on mixed nitrate precursors. The films are epitaxial without any second phase. TEM micrographs show that all of these films have pores with sizes ranging from 5 to 30 nm. Grain boundaries are not observed. Selected area diffraction shows that the films are single-crystal-like, despite the porosity. All the films are smooth and crack-free.

The precursors first decompose into an amorphous mixture. Heterogeneous nucleation occurs on the lattice-matched single-crystal substrate surface. The epitaxial films grow upward and consume the amorphous regions. The crystallization temperature of LaAlO $_3$ is lower for thin films than for bulk samples due to nucleation on the substrate. The crystallization of LaAlO $_3$ does not exhibit linear growth kinetics. The Johnson-Mehl-Avrami exponent of growth is between 1.4 to 1.5. This deviation from the linear growth model (n = 1) can be attributed to continuous nucleation on the substrate/film interface.

Order No.: JA705-020 © 1997 MRS

Phase formation in molybdenum disilicide powders during in-flight Induction plasma treatment

X. Fan, T. Ishigaki, Y. Sato

(National Institute for Research in Inorganic Materials)

The in-flight modification of $MoSi_2$ powders has been carried out by using an Ar-H $_2$ induction plasma. Reactor pressure, powder feed rate and plate power level were taken as the experimental parameters to alter the thermal history of the injected powder particles. Metastable hexagonal structure of β -MoSi $_2$ is the major phase observed in the Ar-H $_2$ induction plasma treated molybdenum disilicide powders, while the stable phase of tetragonal structure of α -MoSi $_2$ usually retains no less than 30 wt.%. Deapending on the experimental condition and the deviation from stoichiometry in raw materials, low silicides, Mo_5Si_3 and Mo_3Si , and free Si were observed.

Order No.: JA705-021 © 1997 MRS

Phase-formation kinetics of xerogel and electrical properties of sol-gel-derived $Ba_xSr_{1-x}TiO_3$ thin films

S-I. Jang, B-C. Choi, H.M. Jang

(Pohang University of Science and Technology)

Chemically homogeneous $Ba_xSr_{1-x}TiO_3$ (BST with x=0.6) multi-component sol was synthesized using barium oxide, strontium chloride, and Ti-alkoxide (titanium isopropoxide) as starting materials. Acetylacetone (AcAc) was introduced as a chelating agent to reduce a rapid

hydrolysis rate of Ti-alkoxide. Analysis of FTIR spectra indicated that the stabilization of BST sols was achieved by the chelation of Ti-alkoxide with the enolic form of AcAc. The effective activation energy associated with the formation of perovskite phase from the xerogel was estimated by the DTA experiment using various heating rates. It is approximately 400 kJ/mol with the Avrami exponent (reaction order) of n = 1, suggesting that the growth of perovskite BST is diffusion-controlled. The calculated half-life time suggests that the minimum temperature for the crystallization which is practically accessible to a real processing is approximately 600°C . The BST thin film fabricated on the "Pt(150 nm)/Ti(100 nm)/ SiO_2(100 nm)/Si" substrate exhibited the relative dielectric permittivity of 310 and can be represented by an equivalent circuit consisting of a resistive component originated from the bulk perovskite grain and a parallel RC component resulting from the presence of the grain boundary.

Order No.: JA705-022 © 1997 MRS

The ballistic failure mechanisms and sequence in semi-infinite supported alumina tiles

D. Sherman, D.G. Brandon

(Technion-Israel Institute of Technology)

The basic ballistic failure mechanisms and their sequence occurring in dense alumina tiles during projectile penetration were investigated. The alumina tiles were supported by semi-infinite support blocks made of three different materials. Initially, a drop weight test (DWT) was used to gain an insight into the damage mechanisms and sequence during quasi-static impact conditions. The quasi-static damage mechanisms were compared with the damage obtained in 0.3 cal. armor piercing tests (APT).

The DWTs results suggested the following sequence of quasi-static failure mechanisms: radial tensile cracks, associated with the low tensile strength of the ceramic formed initially, as a result of the bending induced by local deformation at the opposing surface. Subsequently, a shear dominated cone crack propagated from the edge of the contact zone. If sufficient energy was available, crushing of the material beneath the contact zone developed during the final stages of failure. It is shown that these so-called "quasi-static" damage mechanisms, identified from the DWTs also corresponded to the damage mechanisms and sequence during APTs.

Order No.: JA705-023 © 1997 MRS

Hot filament assisted diamond growth at low temperatures with oxygen addition

Z.L. Tolt*, L. Heatherly*, R.E. Clausing*, C.S. Feigerle* (*Oak Ridge National Laboratory, *University of Tennessee)

Addition of a small amount of oxygen to the CH₄ and H₂ feed gas permits hot filament assisted chemical vapor deposition (HFCVD) of diamond at significantly lower filament and substrate temperatures. The former can be reduced to as low as 1400°C and the latter to 450°C. The amount of oxygen required is much lower than what has been used in most studies of the oxygen effect. For each CH₄%, there is a narrow window in the O/C ratio, where diamond can be deposited at low temperature. This window shifts to higher O/C ratios as the CH₄% increases and expands with increases in filament temperature. The effects of changing substrate and filament temperatures on growth rate and film quality are often not consistent with previous experiences with HFCVD of diamond. Increasing the filament temperature does not always improve the growth rate and film quality, and the non-diamond carbon content in the film is dramatically reduced at lower substrate temperatures. Optimum conditions were found that gave reasonable growth rates (~0.5 µm/h) with high film quality at filament temperatures below 1750°C and substrate temperatures below 600°C. With these reductions in operating temperatures, power consumption can be significantly reduced and the filament lifetime extended indefinitely.

Order No.: JA705-024 © 1997 MRS

Nucleation and growth of oriented diamond on Si(100) by biasassisted chemical vapor deposition

M. Nishitani-Gamo*+#, T. Ando*+, K. Yamamoto*, P.A. Dennig*, Y. Sato* (*National Institute for Research in Inorganic Materials, *Japan Science and Technology Corporation, *Toppan Printing Co., Ltd.)

In order to clarify the effect of bias treatments on the highlyoriented growth of diamond, we investigated the relation between the
silicon surface morphology changes after applying a bias voltage, and the
orientation of the diamond crystallites after growth. We report two major
findings. First, a textured structure on the Si surface after the bias pretreatment was found to be a necessary but insufficient indicator for the
subsequent growth of highly-oriented diamond. Second, although bias
pretreatments effectively enhance nucleation, we did not find a clear
relationship between the nucleation density and the percentage of
oriented crystallites. The highest nucleation densities resulted in randomlyoriented films. We conclude that bias pretreatments affect the nucleation
enhancement and the diamond orientation through different mechanisms.

Order No.: JA705-025

Nitrogen plasma source ion implantation for corrosion protection of aluminum 6061-T4

J.H. Booske, L. Zhang, W. Wang, K. Mente, N. Zjaba, C. Baum, J.L. Shohet

(University of Wisconsin-Madison)

It is established that nitridation of aluminum (AI) 6061-T4 by plasma source ion implantation (PSII) can dramatically enhance the pitting corrosion resistance of this alloy in marine environments (i.e., chlorine-ion-bearing aqueous solutions or humid atmospheres). Corrosion tests and microstructure analyses establish that the mechanism for successful passivation against chloride-induced pitting corrosion involves the formation of a multilayered microstructure, including the presence of a continuous layer of aluminum-nitride (AIN). Important process variables are the implantation voltage and the nitrogen dose (or total implantation time), as these two variables establish the implanted nitrogen concentration. Too high or too low an implanted nitrogen concentration will not yield the continuous AIN layer required for good cor-rosion resistance. PSII is attractive for this application as it provides for uniform, conformal implantation of irregularly shaped objects without masking, beam rastering, or object rotation.

Order No.: JA705-026

© 1997 MRS

Excess Li ions in a small graphite cluster

M. Nakadaira*, R. Saito*, T. Kimura*, G. Dresselhaus+, M.S. Dresselhaus+

(*University of Electro-Communications, +Massachusetts Institute of Technology)

We calculate the optimized geometry and the corresponding electronic structure of Li ions doped in a small graphite cluster with dangling bonds or hydrogen terminations at the edge surrounding the cluster. The calculations imply both covalent and ionic bonds of Li ions to carbon atoms, which may be relevant to explaining the broad signal of the ⁷Li NMR Knight shift spectra. Li intercalation, in particular, is possible even at the hydrogen-terminated edges. Because of the finite size effect of the cluster, the ionicity of intercalated Li ions has a large distribution of values, ranging from positive values close to that in graphite intercalation compounds to even slightly negative values, depending on the bonding geometry. We propose that the cluster edge surface plays a special role in accommodating excess Li ions in the disordered graphitic system.

Order No.: JA705-027

Surface and bulk characterization of Rh/ZrO_2 prepared by absorption of $Rh_a(CO)_{12}$ clusters on ZrO_2 powder

L.E. Depero*, R. Bertoncello+, T. Boni#, P. Levrangi*, I.N. Sora*, E. Tempesti*, F. Parmigiani§

(*University of Brescia, *University of Padua, *CISE, \$Polytechnic of Milan)
Rh nanoparticles supported on ZrO₂ powder were prepared by
adsorbing Rh₄(CO)₁₂ clusters from hexane solution under Ar atmos-

phere. Four samples with Rh content ranging from 0.25 Rh %wt up to 4.10 Rh %wt are studied by x-ray diffraction (XRD), transmission electron microscopy (TEM), x-ray photoelectron spectroscopy (XPS), scanning Auger microscopy (SAM) and time-of-flight secondary ion mass spectroscopy (ToF-SIMS).

TEM measurements show, for all the samples, Rh particles with a size of about 50 Å. The 4.10 Rh %wt sample show also some agglomerates of Rh nanoparticles, and only for this sample Rh metallic phase was detected by XRD. The profile analysis of the XRD lines indicate an average size of the Rh crystallites of about 60 Å.

XPS studies show only a single spectral component for the Zr3d $_{5/2}$ core line at 182.2 eV. Instead, at least two components at 307.2 eV and 308.5 eV are detected for the Rh3d $_{5/2}$ core line. These results suggest that Zr is present only as oxidized state, whereas non-oxidized and oxidized Rh are both observed. A non-oxidized Rh state is also suggested by the XPS valence band electron removal spectrum which exhibits a significant emission within the Zr0 $_2$ band gap assigned to Rh4d t_{2g} and t_{2g} and t_{2g} orbitals. A further support to this finding arises from scanning Auger maps of t_{2g} Rh t_{2g} where non-oxidized Rh is observed.

Finally scanning Auger maps using the O_{KVV} and the Zr $M_{45}N_{23}V$ emissions show surface regions where only the Zr Auger lines are detected, whereas on pure ZrO_2 powder this effect is not observed. Since it is possible to rule out from the XPS Zr3d core line spectra the presence of metallic zirconium hydrogen spillover mechanisms are invoked to explain these results.

Order No.: JA705-028

© 1997 MRS

Vapor-deposited CaWO₄ phosphor

P.F. Carcia, M. Reilly, C.C. Torardi, M.K. Crawford, C.R. Miao, B.D. Jones (DuPont Central Research and Development)

In this paper we describe the preparation, microstructure, and x-ray excited luminescence of vapor-deposited $CaWO_4$ films up to about 50 μm thick, comparing them to particulate $CaWO_4$ phosphor screens, used in medical diagnostic imaging. Films that we e-beam evaporated on substrates heated at or above $500^{\circ}C$ were polycrystalline with the scheelite structure, while on unheated substrates, films were initially amorphous but became crystalline after annealing them in air above about $750^{\circ}C$. Crystalline $CaWO_4$ films irradiated with x-rays produced light emission peaked at 430 nm. The emission intensity depended on film thickness and grain size and was comparable to particulate $CaWO_4$ phosphor screens. Because the vapor deposited films also exhibited superior resolution, they are promising for diagnostic x-ray imaging.

Order No.: JA705-029 © 1997 MRS

Effect of lattice mismatch on the epitaxy of sol-gel LiNb0₃ thin films T.A. Derouin, C.D.E. Lakeman, X.H. Wu, J.S. Speck, F.F. Lange (University of California-Santa Barbara)

A solution precursor method based on metal alkoxides was used to produce epitaxial LiNbO $_3$ thin films, ~200 nm thick, on (0001) sapphire substrates. Transmission electron microscopy revealed that the major cause of surface roughness in these films was grain boundary grooves between mosaic grains with misorientations $\leq 5^{\circ}$. It is postulated that these low angle boundaries directly result in surface grooving and roughness. The epitaxial films also contained two distinguishable variants in the film/substrate interfacial plane, namely, an aligned variant, $<1210>_{\text{LiNbO}_3}$ II $<1210>_{\text{Al2O}_3}$ and a 60° rotated variant, $<1210>_{\text{LiNbO}_3}$ II $<1210>_{\text{Al2O}_3}$ and a 60° rotated variant, $<1210>_{\text{LiNbO}_3}$ II $<1210>_{\text{LiNbO}_3}$ method was used to minimize the presence of the 60° rotated variant. An epitaxial buffer layer of Fe₂O₃ was used to lower the mismatch strain, eliminate the 60° rotated variant, and reduce the mosaic nature of the LiNbO $_3$ film. X-ray rocking curve full width at half maximum (FWHM) values measured on the (0112) film peak indicate that the mosaic character can be reduced from 1.5° to 0.76° by using a buffer layer.

Order No.: JA705-030

© 1997 MRS

Lattice site and photoluminescence of erbium implanted in α -Al₂O₃ G.N. van den Hoven*, A. Polman*, E. Alves*, M.F. da Silva*, A.A. Melo*, J.C. Soares*

(*FOM-Institute for Atomic and Molecular Physics, +ITN, *Centro de Física Nuclear da Universidade de Lisboa)

Single-crystal sapphire $(\alpha\text{-}Al_2O_3)$ was implanted at room temperature with 200 keV erbium ions to a fluence of 8 x 10^{13} cm^{-2}. Ion channeling using 1.6 MeV He^+ shows that the crystal suffers little damage for this low dose implant. Angular scans through axial and planar directions in the crystal indicate that 70% of the Er atoms reside on displaced octahedral sites in the $\alpha\text{-}Al_2O_3$ lattice. As pure Al_2O_3 has a high density of free octahedral sites, this explains why high concentrations of Er can be dissolved in this material. Smaller fractions of Er are found on tetrahedral (20%) and random (10%) sites. The samples exhibit strongly peaked photoluminescence spectra around 1.5 μm , due to intra-4*f* transitions in Er³+, indicating the existence of well-defined sites for the luminescing Er³+ ions. It is concluded that the octahedral site is the dominating optically active site in the lattice.

Order No.: JA705-031 © 1997 MRS

Spectroscopic study of Na-TCNQ in a poly (ethylene oxide) matrix [TCNQ = 7,7',8,8' tetracyanoquinodimethane]

A. Arena*, G. Di Marco+, M. Lanza+, S. Patané*, G. Saitta* (*Istituto Nazionale per la Fisica della Materia, +Istituto di Tecniche Spettroscopiche-CNR)

X-ray photoelectron spectroscopy (XPS) and optical studies have been performed on P(EO)_n-Nal-TCNQ (n = 1, 10) systems, obtained by

means of a solid state reaction technique. The electron spectroscopy, the absorption in the ultraviolet-visible-near infrared range, and the infrared transmission findings allow us to conclude that the interaction between the polymer, the iodide and the electron acceptor molecule results in the formation of the ion-radical salt Na-TCNQ and in the oxidation of I^- to the metallic state. The presence within the examined specimens of crystalline and amorphous phases has been confirmed by the results of differential scanning calorimetry (DSC) measurements. The optical, electronic and thermal properties of the $P(EO)_n$ -NaI-TCNQ mixtures have then been correlated to the results of preliminary a.c. electrical transport investigations. **Order No.: JA705-032**

Agglomeration of silica spheres under ultrasonication

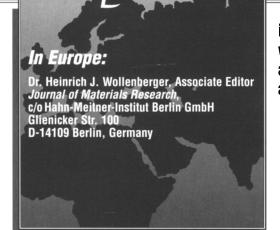
N. Enomoto, S. Maruyama, Z. Nakagawa (Tokyo Institute of Technology)

Power ultrasound of 20 kHz was applied to the synthesis of silica spheres via the controlled hydrolysis of tetraethoxysilane (TEOS). Silica spheres of about 0.3 μm were agglomerated to form tolerably uniform, dense particles of about 2 μm through 90 mins sonication. This agglomeration behavior was examined by laser diffraction particle size analysis and transmission electron microscopy. It was found that the agglomeration process involves (i) incubation period where no agglomeration occurs, (ii) rapid formation of ramified particles, and (iii) their densification. It was inferred that sonication enhances the collision among silica spheres.

Order No.: JA705-033 © 1997 MRS

Please use the convenient postcard located in the back of the MRS Bulletin to order JMR reprints. When ordering single article reprints please note they are not available until the issue is published. See JMR Abstracts on the MRS Website at http://www.mrs.org/publications/jmr/jmra/.

Did you know...



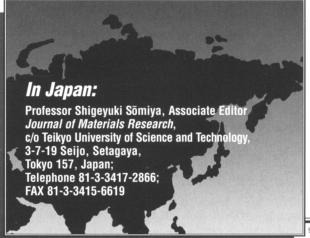
Guidelines for submitting to *JMR* can be found on the inside front cover of each issue, on the MRS Homepage, or contact:

Journal of Materials Research.

Editorial Office, 9800 McKnight Road, Pittsburgh, PA 15237; Telephone (412) 367-9111; FAX (412) 367-4373. E-mail: jmr@mrs.org

Our address on the Worldwide Web is: http://www.mrs.org/

in addition to the Editorial Office in the U.S.A., we have one Associate Editorial Office in Europe and one in Japan. Submissions are welcome at any office.



960705